# PMS activation using reduced graphene oxide under sonication: Efficient metal-free catalytic system for the degradation of rhodamine B, bisphenol A, and tetracycline

Yacine Cherifi, Ahmed Addad, Hervé Vezin, Alexandre Barras, Baghdad Ouddane, Ahcène Chaouchi, Sabine Szunerits, Rabah Boukherroub

# PMS activation using reduced graphene oxide under sonication: Efficient metal-free catalytic system for the degradation of rhodamine B, bisphenol A, and tetracycline

Yacine Cherifi,[1,2] Ahmed Addad,[3] Hervé Vezin,[4] Alexandre Barras,[1] Baghdad Ouddane,[4] Ahcène Chaouchi,[2] Sabine Szunerits,[1] Rabah Boukherroub[1*]

[1]*Univ. Lille, CNRS, Centrale Lille, ISEN, Univ. Valenciennes, UMR 8520 - IEMN, F-59000 Lille, France*

[2]*Laboratoire de Chimie Appliquée et Génie Chimique de l'Université Mouloud Mammeri de Tizi-Ouzou, Algérie*

[3]*Univ. Lille, CNRS, UMR 8207 – UMET, F-59000 Lille, France*

[4]*Univ. Lille, UMR CNRS 8516-LASIR Laboratoire de Spectrochimie Infrarouge et Raman 59655 Villeneuve d'Ascq, France*

*To whom correspondence should be addressed: rabah.boukherroub@iemn.univ-lille1.fr

**Abstract**

This study addresses the influence of ultrasound irradiation on the activation of peroxymonosulfate (PMS) using reduced graphene oxide (rGO) under metal-free conditions for the catalytic degradation of rhodamine B (RhB), bisphenol A (BPA) and tetracycline (TC). Our results revealed that the combination of PMS/rGO and ultrasonication enhanced significantly the degradation rate, reaching full degradation in relatively short times with total organic carbon (TOC) removal exceeding 85% of the investigated pollutants. In contrast, under these experimental conditions, rGO/ultrasound and PMS/ultrasound achieved less than 20% degradation of the same pollutants. Electron paramagnetic resonance (EPR) studies along with quenching experiments suggested that hydroxyl radicals ($^{\bullet}$OH) are the dominant reactive species in the degradation process. Furthermore, inductively coupled plasma atomic emission spectroscopy (ICP-AES) and EPR data revealed the presence of trace manganese (Mn) in rGO. To elucidate the role of Mn on the degradation process, rGO was subjected to hot acid treatment for 48 h to remove trace Mn. While the chemical composition of rGO was not significantly altered by this chemical treatment, the degradation efficiency decreased upon Mn dissolution. The result suggests that trace metal in rGO might account for the efficiency of PMS activation. Finally, plausible degradation pathways were proposed based on LC-MS analysis of the reaction intermediates.

***Keywords:*** *Reduced graphene oxide; PMS; Ultrasonication; Rhodamine B; Bisphenol A; Tetracycline; Degradation mechanism.*

## 1. Introduction

The release of organic pollutants from some industrial wastewaters in environment represents a major issue encountered worldwide, because of the potential transformation of these molecules into harmful species to humans and the environment. In this context, efficient separation/removal of organic pollutants from water is of paramount importance. Many methods have been applied for efficient removal or degradation of organic pollutants from wastewaters, including adsorption [1], coagulation [2], biological treatment [3], electrochemical [4, 5] and advanced oxidation processes (AOPs) [6, 7]. Among AOPs, Oxone (peroxymonosulfate, PMS) activation using transition metals has found widespread applications in environmental remediation, because of the high oxidation potential (2.5 - 3.1 V) of the generated $SO_4^{\bullet-}$ radicals involved in the degradation process [7]. This approach permitted to remove recalcitrant pollutants where $^{\bullet}OH$ radicals failed to or were not powerful enough to achieve efficient degradation [7].

While PMS activation has been mainly achieved using metal ions (M=Fe, Ni, Co, Mn), Sun *et al.* [8] demonstrated that reduced graphene oxide (rGO) can act as an efficient activating material of PMS to generate sulfate radicals ($SO_4^{\bullet-}$). Interestingly, rGO proved to be more efficient than other carbon allotropes, including the parent graphene oxide (GO), graphite, activated carbon, and multiwall carbon nanotubes, and even more than $Co_3O_4$ for the degradation of methylene blue (MB), phenol, and 2,4-dichlorophenol (DCP) in water [8]. Although this study represents an interesting starting point for PMS activation under metal-free conditions to produce $SO_4^{\bullet-}$ radicals, the mechanism of activation is still not clear. Following this study, Liu *et al.* prepared porous and metal-free rGO materials through physical ($CO_2$), chemical ($ZnCl_2$) or physico-chemical ($CO_2$/$ZnCl_2$) activation and investigated their efficacy for dye (MB) adsorption and degradation by PMS activation [9].

The results revealed that porous rGO, obtained through physical activation, was more efficient for PMS activation and MB degradation.

Ultrasound activation was proposed as an effective and viable advanced oxidation process (AOP) for the degradation of organic pollutants [10]. One of the basic concepts of sonochemistry is the generation of free radicals induced by cavitation of microbubbles formed upon ultrasound irradiation [11]. As a consequence, ultrasound irradiation is often applied to increase the degradation rates of organic pollutants under various conditions. For example, it was recently demonstrated that cresol red (CR) removal from water can be achieved under ultrasound irradiation (300 kHz) in acidic medium [12]. The degradation was power dependent with a maximum removal being reached at 80 W. Interestingly, addition of Oxone improved significantly the sonolytic degradation of CR [12].

The combination of ultrasound and semiconductor materials or metal ions such as samarium-doped ZnO [13], $TiO_2$ [14], $Er^{3+}$:$YAlO_3$/$TiO_2$–$SnO_2$ [15], ZnO/graphene/$TiO_2$ [16], $Co_3O_4$ [17], magnetic cobalt-graphene (MCG) [18], Zeolitic Imidazole Framework-67 (ZIF-67) [19], Fe–Co/SBA-15 [20], GO-$Fe^{3+}$ hybrid [21], $Co^{2+}$ [22], in absence or presence of Oxone (peroxymonosulfate) has been successfully applied for the degradation of various organic pollutants. The addition of Oxone (PMS) improved the degradation rate for all investigated systems.

In the present study, we investigated PMS activation using reduced graphene oxide (rGO) under ultrasound irradiation for the degradation of various pollutants such as rhodamine B (RhB), bisphenol A (BPA) and tetracycline (TC) at room temperature. Under optimized conditions, the PMS/rGO system allowed full decomposition of the pollutants in relatively short times with total organic content removal exceeding 85%. While the combination of ultrasound/semiconductor to activate PMS for the degradation of organic pollutants has been studied in many reports, to the best of our knowledge, rGO/PMS system performance under

ultrasound irradiation has not yet been reported. Furthermore, removal of metal (Mn) contamination, commonly introduced during extensive oxidation of GO using $KMnO_4$, in rGO decreased the degradation rate, suggesting the participation of the metal contamination in the degradation process. Finally, LC-MS was performed to determine the intermediate reactive species involved in the degradation process.

## 2. Experimental Section

### 2.1. Materials and methods

All chemicals and reagents were of analytical grade and used without any purification. Hydrazine, rhodamine B (RhB), bisphenol A (BPA), tetracycline (TC), 5,5-dimethyl-1-pyrroline N-oxide (DMPO), nitric acid ($HNO_3$), and sulfuric acid ($H_2SO_4$) were obtained from Sigma-Aldrich (France).

The water used throughout the experiments was purified with a Milli-Q system from Millipore Co. (resistivity = 18 MΩ.cm).

Graphene oxide (GO) powder was purchased from Graphenea (Spain).

### 2.2. Preparation of reduced graphene oxide (rGO)

In a typical procedure, GO (100 mg) was loaded into a 250-mL round bottom flask and water (100 mL) was then added, yielding an inhomogeneous yellow-brown dispersion. This dispersion was sonicated until it became clear with no visible particulate matter. Hydrazine hydrate (1.00 mL, 32.1 mmol) was then added and the solution heated in an oil bath at 80 °C under a water-cooled condenser for 12 h over which the reduced GO gradually precipitated out as a black solid. This product was isolated by filtration over a medium fritted glass funnel, washed copiously with water (5 × 100 mL) and methanol (5 × 100 mL), and dried on the funnel under a continuous air flow.

### 2.3. Catalytic oxidation procedure

The course of pollutant (RhB, BPA or TC) degradation was analyzed using a Bio-UVmc² spectrophotometer (Safas, Monaco) in the 200-800 nm wavelength range at ambient temperature (25 °C). A given amount of PMS ($2KHSO_5 \cdot KHSO_4 \cdot K_2SO_4$) was added to the pollutant aqueous solution, followed by addition of a known quantity of catalyst to initiate the reaction. The reaction mixture was subjected to ultrasonication at 35 kHz (Fischer Bioblock Scientific, power: 240 W). The degradation reaction course was monitored by means of UV–vis spectrophotometry. All experiments were performed in triplicate.

The stability of rGO catalyst was assessed through recycling experiments for the degradation of RhB (20 µM) in the presence of catalyst (1 mg/mL) and PMS (0.3 mM) under ultrasonication (35 kHz). After each cycle, a fresh concentrated solution of RhB was added to the solution to obtain an initial concentration of RhB (20 µM).

## 3. Results and discussion

### *3.1. Preparation and characterization of reduced graphene oxide (rGO)*

The reduced graphene oxide (rGO) investigated in the present work was prepared by hydrazine reduction of commercially obtained graphene oxide (GO). **Figure 1a** depicts the UV-vis absorption spectra of GO before and after reduction with hydrazine. It comprises the characteristic bands at 227 and 310 nm due to π-π* and n-π* transitions, respectively. The band at 227 nm is attributed to the C=C bonds in the aromatic domains, while the band at 310 nm is assigned to the C=O transitions of the carbonyl groups located in the edges of the GO sheets. After reaction with hydrazine, a shift to 270 nm was observed, indicating the formation of larger $sp^2$ domains in the material.

X-ray diffraction (XRD) analysis further confirms the reduction process through the obvious shift of the diffraction peak due to the (002) plane at $2\theta$ value of 10° for GO to 22° for rGO (**Fig. S1**).

**Figure S2** displays the FTIR spectra in transmission mode of GO before and after reaction with hydrazine. The FTIR spectrum of GO comprises several bands at 3300, 1732, 1584, 1232, and 1060 $cm^{-1}$. The band at 3300 $cm^{-1}$ is attributed to the stretching vibration of surface hydroxyl (-OH) groups and/or intercalated water, while the other bands are ascribed to C=O stretching vibration (1732 $cm^{-1}$), vibration of unoxidized graphite domains (1584 $cm^{-1}$), and stretching vibrations of oxygen-containing groups (C-OH and alkoxy C-O stretching vibrations at 1225 and 1057 $cm^{-1}$, respectively). Upon GO reduction with hydrazine, the stretching vibrations due to oxygen containing groups decreased significantly and the peak due to $Csp^2$ vibration is shifted to 1568 $cm^{-1}$, suggesting the restoration of the graphenic network in rGO [23].

Raman spectroscopy is a common technique used to characterize graphenic materials. **Figure 2** depicts the Raman spectra of GO before and after reduction with hydrazine. The Raman spectrum of GO consists of two peaks at 1367 and 1589 $cm^{-1}$ ascribed respectively to the D and G bands [23, 24]. The D-band is associated with defects and disorder in the graphenic network, while the G-band is ascribed to $sp^2$-bonded carbon atoms in the 2-dimensional hexagonal lattice. The ratio ($I_D/I_G$) of D band ($A_{1g}$ mode breathing vibration) to G band ($E_{2g}$ vibrational mode) intensity is commonly used to determine the degree of disorder in carbon materials. The $I_D/I_G$ intensity ratio is 0.84 for GO (**Table S1**). After GO reduction with hydrazine, a blue-shift of the D- and G-bands to 1356 and 1583 $cm^{-1}$, respectively, was observed along with an increase of the $I_D/I_G$ intensity ratio to 1.05. The increase of the $I_D/I_G$ ratio is an indication that the average size of the $sp^2$ domains decreased

during hydrazine reduction, while their number increased in rGO as compared to GO, which is in full agreement with previous reports [24, 25].

X-ray photoelectron spectroscopy (XPS) was performed to examine the chemical composition of GO before and after hydrazine reduction. Typical XPS survey spectra of rGO are illustrated in **Figure S3**. They both comprise peaks ascribed to $C_{1s}$, $N_{1s}$ and $O_{1s}$ at 283, 399 and 531 eV, respectively. The high resolution XPS spectrum of the $C_{1s}$ region of GO is displayed in **Figure S4**. It can be fitted with four components at 284.6, 286, 287 and 288.5 eV ascribed to $Csp^2$, C-O bonds in hydroxyl and epoxy groups, C=O and -COOH groups, respectively [25]. The high resolution XPS spectrum of the $C_{1s}$ region of rGO is depicted in **Figure 3(a)**. It can be deconvoluted into several components at 284.4, 285.4, 286.5 and 288.2 eV ascribed to $Csp^2$, C-H/C-C, C-O, and COOH groups, respectively. The small peak at 291.1 eV is due to the $\pi$–$\pi^*$ shake-up satellite [25].

The morphology, microstructure and chemical composition of rGO were further examined using high-resolution transmission electron microscopy (HRTEM) and energy-dispersive X-ray (EDX) spectroscopy (**Fig. 4**). HRTEM analysis confirmed the formation of a few graphene sheets with crumbled-like morphology. EDX analysis confirmed that rGO was essentially composed of a main carbon peak along with a minor oxygen contribution, in accordance with XPS analysis.

*3.2. Degradation of Rhodamine using rGO/PMS under ultrasonication*

We have next investigated the performance of rGO for PMS activation under ultrasonication for the degradation of various pollutants, including rhodamine B (RhB), bisphenol A (BPA), and tetracycline (TC). For an efficient catalytic process, the catalyst should be stable under the operating conditions. We thus characterized rGO that has been subjected to ultrasonication for 3 h in presence of 0.3 mM PMS. Raman analysis showed a

red-shift of the D- and G-bands frequency by about 5 $cm^{-1}$ as compared to rGO, while the $I_D/I_G$ ratio was not affected significantly (1.05 for rGO and 1.08 after PMS treatment for 3 h under ultrasonication), **Table S1**. Additionally, XPS analysis revealed a slight oxidation of rGO (**Table S2**). From these results, it was evident that rGO was stable under our experimental conditions and can be further investigated for catalytic processes.

The reaction was first optimized using RhB (20 µM), rGO (0.25 mg/mL) and PMS (0.3 mM). Several controls have been recorded to assess the beneficial effect of ultrasound on the catalytic oxidation of RhB. While ultrasonication alone (in absence of PMS) did not show any degradation of RhB, addition of rGO alone led to RhB adsorption (10%). In absence of rGO, addition of PMS (0.3 mM) to RhB (20 µM) induced 12% degradation without ultrasonication; the degradation reached almost 28% upon ultrasonication of the RhB/PMS mixture. When rGO (0.25 mg/mL) was added to a mixture of RhB (20 µM) and PMS (0.3 mM), about 15% of RhB was degraded. This contrasts with the full degradation achieved after 15 min under ultrasonication (**Fig. 5**).

The influence of rGO loading and PMS concentration on RhB degradation under ultrasonication was examined (**Fig. 6**). The catalytic effect of rGO loading (0.25 and 0.5 mg/mL) on RhB (20 µM) degradation in presence of PMS (0.3 mM) under ultrasonication is illustrated in **Fig. 6A**. While there is a clear difference in the degradation rate in the first 10 min, a full degradation of RhB was achieved after 15 min ultrasonication for both rGO loadings. From these results, it was concluded that rGO loading of 0.25 mg/mL is sufficient for this catalytic process. Next, the effect of PMS concentration (0.1, 0.2 and 0.3 mM) on the degradation of RhB (20 µM) catalyzed by rGO (0.25 mg/mL) under ultrasonication was evaluated (**Fig. 6B**). Increasing PMS concentration from 0.1 to 0.3 mM resulted in a clear decrease of the degradation time from 45 to 20 min, suggesting that 0.3 mM of PMS is sufficient to drive the degradation reaction to completion. Additionally, the influence of the

pH on RhB degradation was investigated (**Fig. S5**). The degradation of RhB (20 µM) using 0.25 mg/mL of rGO and 0.3 mM of PMS under ultrasonication was assessed at different pH values (3, 5, 6.4, 7, 8, 10). The results clearly revealed that the pH had a negligible effect on RhB degradation under our experimental conditions.

The optimized conditions (rGO=0.25 mg/mL, PMS=0.3 mM, pH=6.4), established from the above data, were applied for the removal of different amounts of RhB (20, 30, and 40 µM) under ultrasonication. It can be seen that upon increasing the RhB concentration, the time required to reach its full degradation increased from 20 to 40 min for 20 µM and 40 µM, respectively (**Fig. 6B**). The performance of rGO under ultrasonication is comparable to or even better than that reported for various metal/PMS systems with the advantage of operating under metal-free conditions (**Table S3**). Interestingly, TOC analysis revealed that about 86% of RhB was mineralized within 20 min under ultrasonication using rGO (0.25 mg/mL)/PMS (0.3 mM) system (**Fig. 7**). The result suggests that RhB was not only decomposed into small molecules, but completely mineralized using this process, in accordance with UV-vis absorption analysis.

The stability of any catalytic system is an important aspect for any further development and/or implementation for practical applications. The stability of rGO/PMS system for RhB degradation was evaluated through cycling experiments. **Figure 8** illustrates the performance of rGO (0.25 mg/mL)/PMS (0.3 mM) for the catalytic degradation of RhB (20 µM) under ultrasonication (36 kHz, 200 W). No obvious change of the full degradation time was observed up to 7 cycles; thereafter, the degradation time increased slightly to reach 30, 35 and 50 min for the 8, 9, and 10 cycles. The data clearly indicates the good stability of the rGO/PMS system for RhB degradation under ultrasonication.

To gain some insights on the plausible reaction mechanism and potential intermediates involved in the catalytic degradation of RhB by rGO/PMS system under ultrasonication,

quenching experiments were performed using ethanol (EtOH) and *tert*-butanol (TBA) as quenchers. While EtOH quenches both hydroxyl ($HO^{\cdot}$, $k_{HO^{\cdot}}$ = 1.2-1.8 × $10^9$ $M^{-1}s^{-1}$) and sulfate ($SO_4^{-\bullet}$, $k_{SO4^{-\bullet}}$ = 1.6-7.7 × $10^7$ $M^{-1}s^{-1}$) radicals, TBA scavenges preferentially $HO^{\bullet}$ ($k_{HO^{\bullet}}$ = 6.0 × $10^8$ $M^{-1}s^{-1}$) but much less $SO_4^{-\bullet}$ ($k_{SO4^{-\bullet}}$ = 4 × $10^5$ $M^{-1}s^{-1}$) radicals [26, 27]. **Figure 9** depicts the results of the reaction of RhB (20 µM) with rGO (0.25 mg/mL) and PMS (0.3 mM) under ultrasonication in absence or presence of $HO^{\bullet}$ and $SO_4^{-\bullet}$ scavengers. The results revealed that EtOH inhibited RhB degradation but to less extent than TBA, suggesting that the $HO^{\bullet}$ radicals are the dominant active radical species involved in the degradation process. However, this does not exclude a minor contribution of $SO_4^{\bullet-}$ radicals. Interestingly, the inhibition levels of EtOH and TBA, in the first 5 min, are comparable. This is most likely due to the initial formation of $SO_4^{\bullet-}$ radicals predominantly, followed by $HO^{\bullet}$ radicals formation thereafter.

Additionally, EPR measurements were conducted to identify the active species involved in the degradation of RhB by rGO/PMS under ultrasonication. The EPR spectrum in **Fig. 10** showed that no signal can be detected at room temperature for the rGO material alone. The rGO-PMS exhibited a weak isotropic signal at around g=2.05 with 6 lines features and an hyperfine coupling of 82 G. This signal arises from $Mn^{2+}$ (I=5/2) impurity. Spin trapping experiments by adding DMPO trap agent showed, beside the Mn signal, an intense spin adduct 1 min after addition (**Fig. 11A**). The signals recorded after 10 and 20 min look similar (**Fig. 11B**). The spectra are the superimposition of 2 species. The fourth line with the intensity 1:2:2:1 is due to the trap of $HO^{\bullet}$ radical with its characteristic hyperfine coupling constant $A_N$=$A_H$=14.8G. An additional signal marked with stars arises from an oxidized DMPO species $A_N$= 7.2 G $A_H$=4.1G. In time of course of the reaction from 10 to 20 min, we can clearly see an increase of $HO^{\bullet}$ radical that reached a maximum at 20 min. These results are in good agreement with the quenching experiments.

From these results, a plausible mechanism based on rGO activation of PMS under ultrasonication is believed to take place according to equations (1) and (2). Indeed, rGO as an electron rich material can easily transfer electrons under ultrasonication to generate $SO_4^{-\bullet}$ and $HO^-$ from PMS decomposition (Eq. 1). Subsequent reaction of $SO_4^{-\bullet}$ with $H_2O$ leads to the generation of $HO^\bullet$ radicals (Eq. 2). Both $SO_4^{-\bullet}$ and $HO^\bullet$ radicals are involved in the pollutants' degradation. Even though, $HO^\bullet$ radicals can be potentially generated by direct ultrasonication of the rGO/H2O system, this pathway seems to be less effective under these conditions as less than 40% of RhB is degraded after to 20 min, compared to the full degradation recorded in presence of PMS (**Fig. 5**).

$$HSO_5^- \xrightarrow[))))]{rGO} SO_4^{-\bullet} + HO^- \qquad (1)$$

$$SO_4^{-\bullet} + H_2O \longrightarrow SO_4^{2-\bullet} + HO^\bullet + H^+ \qquad (2)$$

The presence of Mn species in GO and rGO was confirmed by ICP-OES analysis (**Table 1**). The presence of Mn in GO (1.88 wt.%) originates most likely from the oxidation process using $KMnO_4$ during the preparation of GO. Hydrazine reduction was not sufficient to remove Mn species, as evidenced by the presence of comparable amount of Mn (1.89 wt.%) in rGO. It is well-known that $Mn^{2+}$ ions are able to activate PMS to generate reactive species, capable of decomposing organic dyes [28]. To illustrate the role of the residual Mn in rGO on the catalytic process of RhB degradation, rGO was treated with $HNO_3/H_2SO_4$ mixture at 80 °C for 24 or 48 h to remove Mn species. ICP-OES analysis showed a significant decrease of Mn amount to 0.22 and 0.04 wt.% after 24 and 48 h acid treatment, respectively (**Table 1**). Interestingly, the acid-treatment did not induce significant chemical changes as evidenced by Raman (**Fig. S6**) and XPS (**Fig. S7**) analysis. Indeed, Raman analysis showed only a slight decrease of the $I_D/I_G$ ratio to 0.96 for the rGO sample treated with $HNO_3/H_2SO_4$ (1/1) at 80

°C for 24 h, as compared to 1.05 recorded for as-prepared rGO (**Table S1**). Furthermore, XPS data indicated a very limited oxidation of the rGO surface as witnessed by the slight decrease of the C/O ratio from 7.51 (as-prepared rGO) to 6.58 and 6.1 after acid-treatment at 80 °C for 24 and 48 h, respectively (**Table S2**). All these results suggest that the acid-treatment mostly removed Mn species on rGO, but did not induce a considerable change of rGO chemical composition. This is favorable to check the contribution of Mn in the degradation process.

Thus, the catalytic degradation of RhB (20 µM) was investigated using the acid treated rGO (0.25 mg/mL)/PMS (0.3 mM) system under ultrasonication (**Fig. S8**). The result clearly indicated that Mn partial removal slowed down RhB degradation, requiring 35 min ultrasonication to reach complete RhB removal for rGO treated with $HNO_3/H_2SO_4$ at 80 °C for 24 h, as compared to 20 min using as-prepared rGO under otherwise identical experimental conditions. This became more obvious for the acid-treated rGO sample at 80 °C for 48 h where full degradation was not achieved even after 55 min ultrasonication. The results clearly suggest Mn contribution in the degradation process. From XPS analysis, acid treatment induced a slight oxidation of rGO matrix; this also might contribute to a decrease of the degradation rate because GO/PMS system was not as effective as rGO/PMS.

Finally, high performance liquid chromatography (HPLC) was recorded to follow the possible formation of reaction intermediates during RhB degradation using rGO/PMS system under ultrasonication (**Fig. S9**). The chromatograms, recorded at 0, 10 and 20 min, revealed a continuous disappearance of the RhB peak (retention time ~ 13 min) without any evidence for the appearance of new peaks. This clearly indicated that RhB degradation occurred through the destruction of the aromatic network.

*3.3. Degradation of bisphenol A (BPA) using rGO/PMS under ultrasonication*

The efficiency of ultrasound activation of rGO/PMS system was further investigated for other pollutants such as bisphenol A (BPA) and tetracyclin (TC). BPA is an extensively used chemical in the production of polycarbonate plastics and epoxy resins. BPA is known as an anthropogenic endocrine-disrupting compound, which is detrimental for human health and aquatic lives. Thus, it is mandatory to develop effective techniques to remove BPA from contaminated water.

The catalytic degradation of BPA (100 µM) using rGO (0.25 mg/mL) and PMS (1 mM) under ultrasonication was followed by UV-Vis absorption spectrophotometry (**Fig. S10**). A full degradation was attained after 40 min ultrasonication, as witnessed by the disappearance of the characteristic absorption peaks at 225 and 275 nm. The result was furthermore corroborated by TOC analysis revealing about 95% mineralization of TC (**Fig. 7**). Interestingly, BPA degradation was not achieved using rGO, PMS or ultrasonication alone or through the combination of rGO/ultrasonication and PMS/ultrasonication for 40 min (**Fig. 12A**); less than 10% BPA removal was attained under these experimental conditions. The results clearly suggested that the presence of rGO and PMS was necessary to drive BPA degradation to completion.

The effect of dissolved organic and inorganic species on BPA degradation was assessed using humic acid, bicarbonate, nitrate, chloride and phosphate (**Fig. 12B**) [29]. While most of the investigated species did not affect significantly the degradation process, humic acid turned to slow down the degradation rate. This phenomenon might be ascribed to various processes such as humic acid adsorption on the catalyst surface, leading to its partial deactivation [30] or to the participation of humic acid in the catalytic process according to Eqs (1) and/or (2) [29]:

$$\text{Humic acid} + HSO_5^- \rightarrow \text{by-products} + SO_4^{2-} \qquad (1)$$

$$\text{Humic acid} + SO_4^{-\bullet} \rightarrow \text{by-products} + SO_4^{2-} \qquad (2)$$

To further underline the catalytic degradation mechanism of BPA, the reaction intermediates were analysed using LC-ESI-MS in negative mode. As can be seen in **Figure 13**, the chromatograms of BPA after catalytic degradation with rGO/PMS system under ultrasonication display six possible intermediates with retention times at 21.87, 18.54, 16.45, 15.01, 14.54, 12.83 and 8.52 min. MS analysis indicated that the main peak with a retention time of 21.87 min corresponds to BPA (m/z=227), **Fig. S11**. The peak at 18.54 min with $[MH]^-$ m/z 243 is identified as BPA catechol, and was observed at the first stage of the catalytic degradation of BPA. This intermediate is most likely produced through electrophilic attack of $HO^\bullet$ radical onto the aromatic ring of BPA. However, one can exclude its formation *via* electron transfer from BPA to $SO_4^{-\bullet}$ to yield BPA radical cation ($BPA^{+\bullet}$), which in turn reacts quickly with $H_2O$ through hydroxyl abstraction or addition reaction to generate (hydroxyl) BPA radical [31-33]. The peak at 16.45 min (m/z=134) is assigned to 4-(prop-1-en-2-yl) phenol [33-35], while the compound at 14.54 min (m/z=94) is due to phenol molecule [36]. The intermediates with retention times at 12.83 min (m/z=143) and 15.01 min (m/z=167) are attributed to 3,6-dihydroxyhexa-2,4-dienoic acid and 4-(2-hydroxypropan-2-yl)-catechol, respectively [31, 33, 35, 37]. The ion at m/z 82, detected at 8.52 min, can be attributed to penta-1,4-dien-3-one [37].

It is well-known that $SO_4^{-\bullet}$ radical is commonly involved in electron transfer reactions in contrast to $HO^\bullet$ radical, which can participate in hydrogen abstraction or addition reactions [38]. Additionally, $SO_4^{-\bullet}$ is a selective radical that reacts specifically with the aromatic ring, while $HO^\bullet$ can react with both the aromatic ring and the aliphatic chain. Even though $HO^\bullet$ radical is non-selective, the existence of electron-donating OH group in BPA increases the electron density of the aromatic ring, favoring the electrophilic attack of $HO^\bullet$ radical on the

phenyl ring of BPA, to generate intermediate 1 [31, 33, 39]. This was pointed out in a previous study on BPA degradation by different AOPs [31]. The formation of intermediates 2-4 may be rationalized by $HO^{\bullet}$ addition on the BPA phenyl ring followed by C-C bond cleavage and water elimination. Subsequent ring opening leads to the formation of 3,6-dihydroxyhexa-2,4-dienoic acid and penta-1,4-dien-3-one, which could be further mineralized into $CO_2$ and $H_2O$. On the basis of the identified reaction intermediates, a plausible degradation mechanism of BPA by the PMS/rGO system under ultrasonication is schematically illustrated in **Figure 14**. BPA degradation occurred through $HO^{\bullet}$ radical addition, C-C bond cleavage, water elimination and oxidation.

*3.4. Degradation of tetracycline (TC) using rGO/PMS under ultrasonication*

Finally, the efficacy of rGO/PMS system for the removal of tetracycline (TC), a typical antibiotic molecule commonly used for the treatment of infectious diseases in humans and in animal farming, was examined. **Figure 15** summarizes the UV-vis absorption spectra of TC (100 µM) under various experimental conditions. While a simple ultrasonication of an aqueous solution of TC was not effective for its removal, addition of rGO into the solution led to about 20% TC removal. This was improved upon ultrasonication to reach about 40% after 30 min. Interestingly, addition of PMS to TC (100 µM) aqueous solution enhanced its removal to 50% and up to 60% upon ultrasonication for 30 min. The best results were recorded in presence of PMS (1 mM) and rGO (0.25 mg/mL) after 30 min ultrasonication with a complete disappearance of the characteristic absorption peaks of TC (**Fig. S12**). The result was furthermore confirmed by TOC analysis revealing about 91% mineralization of TC (**Fig. 7**).

Similarly, the TC degradation pathways were assessed through LC-ESI-MS. As can be seen in **Figure 16**, TC degradation using PMS/rGO under ultrasonication occurred essentially

in the first 15 min with appearance of several reaction intermediates. The main peak at 11.46 min (m/z=445) of tetracycline was detected and its intensity decreased considerably as the reaction proceeded (**Fig. S13**). The other peaks observed on the MS spectrum of TC are most likely generated according to the following sequence: m/z 445 → m/z 427 (loss of $H_2O$) → m/z 410 (loss of $NH_3$) [40-42]. After reaction of TC with PMS/rGO for 15 min under ultrasonication, new peaks were detected at retention times of 1.98, 2.3, 3.3, 10.1, 21.0, 23.7, 26.3 and 29.3 min. The formation of these intermediates arises from different pathways involving sequential oxidation reactions. Indeed, preferential addition of $HO^{\bullet}$ radical on the C11a-C12 double-bond followed by rearrangement at the C12 position generates the primary intermediate 1 (m/z = 461) [43, 44]. The intermediate 2 detected at m/z=427, referred to as anhydrotetracycline (ATC), is produced *via* a dehydration pathway of TC at the C6 site [45, 46].

Addition of $HO^{\bullet}$ radical on the C2-C3 double bond of primary intermediate 1 leads to the formation of an intermediate 3 with m/z = 477 [44, 46, 47]. While the oxidation of the double bond at C6a-C7 position of the primary intermediate 1 yields intermediate 4 ($m/z = 509$) containing a carboxylic acid group and a ketone group. The intermediate 5 ($m/z = 447$) is formed *via* radical oxidation of $-N(CH_3)_2$ group at C4 site, generating a ketone group. So, we can assume that the intermediate 7 ($m/z = 525$) is produced from 3 through oxidation of the C6a-C7 double bond to form a ketone group and a carboxylic group at position C6a and C7, respectively. Intermediate 7 can be also generated through $HO^{\bullet}$ addition on the C2-C3 double bond of intermediate 4 ($m/z = 509$), producing a hydroxyl and a ketone group respectively at position C2 and C3. Intermediate 6 ($m/z = 491$) is formed by dehydration of intermediate 4 at C6. The intermediate 8 ($m/z = 460$) may be formed *via* oxidation of $-N(CH_3)_2$ of intermediate 6, followed by dehydration referred to an elimination of two $H_2O$ molecules at position C4 and C2. The C10-10a carbon double bond and the amide group at C2 are easily oxidized by

•OH radical to yield intermediates 9 and 10; when the attack takes place at the C10-10a carbon double bond, intermediate 9 (*m/z* = 376) is formed, while upon •OH attack at C2 position, the intermediate 10 (*m/z* = 416) is produced. Oxidation of intermediate 9 by •OH at positions C5a or C11a leads to the formation intermediate 11 (m/z=292) or intermediate 12 (*m/z*=320).

The degradation of intermediate 5 continues may be by the breakage of carbon–carbon single bond to yield intermediate 13 (*m/z*=277), which was also reported by [44, 48]. Then intermediate 13 might be transformed to intermediate 14 (*m/z*=192) *via* loss of methyl and hydroxyl groups and breakage of C–C single bond. The intermediate 15 (*m/z*=136) is produced via hydrogen addition and dihydroxylation, same for intermediate 17 (m/z=133), 2-methylfumaric acid, which might be the last by-products before complete mineralization. Based on the detected reaction intermediates, TC degradation is believed to occur through different pathways as illustrated in **Figure 17**.

## Conclusion

Ultrasound irradiation was utilized to enhance the degradation rate of various organic pollutants such as rhodamine B (RhB), bisphenol A (BPA) and tetracycline (TC) through peroxymonosulfate (PMS) activation in presence of reduced graphene oxide (rGO). This simple and straightforward method takes place under ambient conditions to achieve complete degradation of aforementioned pollutants with high total organic carbon (TOC) removal higher than 85%. Mechanistic studies through quenching experiments and electron paramagnetic resonance (EPR) analysis revealed the dominant role of hydroxyl radicals in the degradation process along with the importance of residual metal traces (Mn) in rGO. Indeed, Mn dissolution in hot nitric acid led to a significant decrease of the degradation rate of RhB under otherwise identical conditions of PMS and ultrasonication. These observations clearly

highlight the influence of trace metals in reduced graphene oxide on its catalytic properties. A plausible mechanism for the degradation of BPA and TC was proposed based on LC-MS analysis.

**Acknowledgments**

The authors gratefully acknowledge financial support from the Centre National de la Recherche Scientifique (CNRS), the Lille University – Sciences and Technology, and the Hauts-de-France region. Yacine Cherifi acknowledges financial support from the Algerian Ministry of Education for a fellowship.

**References**

[1] W. Libbrecht, A. Verberckmoes, J. W. Thybaut, P. Van Der Voort, J. De Clercq, Soft templated mesoporous carbons: Tuning the porosity for the adsorption of large organic pollutants, Carbon, 116 (2017) 528-546.

[2] A. Matilainen, M. Vepsäläinen, M. Sillanpää, Natural organic matter removal by coagulation during drinking water treatment: A review, Adv. Colloid Interface Sci., 159 (2010) 189-197.

[3] M.-K. Henriikka Winkler, C. Meunier, O. Henriet, J. Mahillon, M. Eugenia Suárez-Ojeda, G. Del Moro, M. De Sanctis, C. Di Iaconi, D. G. Weissbrodt, An integrative review of granular sludge for the biological removal of nutrients and recalcitrant organic matter from wastewater, Chem. Eng. J., 336 (2018) 489-502.

[4] F. C. Moreira, R. A. R. Boaventura, E. Brillas, V. J. P. Vilar, Electrochemical advanced oxidation processes: A review on their application to synthetic and real wastewaters, Appl. Catal. B, 202 (2017) 217-261.

[5] E. Brillas, C. A. Martínez-Huitle, Decontamination of wastewaters containing synthetic organic dyes by electrochemical methods. An updated review, Appl. Catal. B, 166-167 (2015) 603-643.

[6] L. Gomathi Devi, R. Kavitha, A review on non metal ion doped titania for the photocatalytic degradation of organic pollutants under UV/solar light: Role of photogenerated charge carrier dynamics in enhancing the activity, Appl. Catal. B, 140-141 (2013) 559-587.

[7] F. Ghanbari, M. Moradi, Application of peroxymonosulfate and its activation methods for degradation of environmental organic pollutants: Review, Chem. Eng. J., 310 (2017) 41-62.

[8] H. Sun, S. Liu, G. Zhou, H. M. Ang, M. O Tadé, S. Wang, Reduced graphene oxide for catalytic oxidation of aqueous organic pollutants, ACS Appl. Mater. Interfaces, 4 (2012) 5466−5471.

[9] S. Liu, W. Peng, H. Sun, S. Wang, Physical and chemical activation of reduced graphene oxide for enhanced adsorption and catalytic oxidation, Nanoscale, 6 (2014) 766-771.

[10] Y. G. Adewuyi, Sonochemistry: Environmental Science and Engineering Applications, Ind. Eng. Chem. Res., 40 (2001) 4681-4715.

[11] L. H. Thompson, L. K. Doraiswamy, Sonochemistry: Science and Engineering, Ind. Eng. Chem. Res., 38 (1999) 1215-1249.

[12] F. Soumia, C. Petrier, Effect of potassium monopersulfate (oxone) and operating parameters on sonochemical degradation of cationic dye in an aqueous solution, Ultrason. Sonochem., 32 (2016) 343-347.

[13] H. Eskandarloo, A. Badiei, M. A. Behnajady, G. M. Ziarani, Ultrasonic-assisted degradation of phenazopyridine with a combination of Sm-doped ZnO nanoparticles and inorganic oxidants, Ultrason. Sonochem., 28 (2016) 169-177.

[14] J. Wang, Y. Guo, B. Liu, X. Jin, L. Liu, R. Xu, Y. Kong, B. Wang, Detection and analysis of reactive oxygen species (ROS) generated by nano-sized $TiO_2$ powder under

ultrasonic irradiation and application in sonocatalytic degradation of organic dyes, Ultrason. Sonochem., 18 (2011) 177-183.

[15] Y. Zhai, Y. Li, J. Wang, J. Wang, L. Yin, Y. Kong, G. Han, P. Fan, Effective sonocatalytic degradation of organic dyes by using $Er^{3+}$:$YAlO_3$/$TiO_2$–$SnO_2$ under ultrasonic irradiation, J. Mol. Catal. A, 366 (2013) 282-287.

[16] P. Nuengmatcha, S. Chanthai, R. Mahachai, W.-C. Oh, Sonocatalytic performance of ZnO/graphene/$TiO_2$ nanocomposite for degradation of dye pollutants (methylene blue, texbrite BAC-L, texbrite BBU-L and texbrite NFW-L) under ultrasonic irradiation, Dyes Pigments, 134 (2016) 487-497.

[17] W. Guo, S. Su, C. Yi, Z. Ma, Degradation of antibiotics amoxicillin by $Co_3O_4$-catalyzed peroxymonosulfate system, Environ. Progress Sustainable Energy, 32 (2013) 193-197.

[18] K.-Y. A. Lin, F.-K. Hsu, W.-D. Lee, Magnetic cobalt–graphene nanocomposite derived from self-assembly of MOFs with graphene oxide as an activator for peroxymonosulfate, J. Mater. Chem. A, 3 (2015) 9480-9490.

[19] K.-Y. Andrew Lin, H.-A. Chang, Zeolitic Imidazole Framework-67(ZIF-67) as a heterogeneous catalyst to activate peroxymonosulfate for degradation of Rhodamine B in water, J. Taiwan Inst. Chem. Eng., 53 (2015) 40-45.

[20] C. Cai, H. Zhang, X. Zhong, L. Hou, Ultrasound enhanced heterogeneous activation of peroxymonosulfate by a bimetallic Fe–Co/SBA-15catalyst for the degradation of Orange II in water, J. Hazard. Mater., 283 (2015) 70-79.

[21] S. Thangavel, N. Raghavan, G. Kadarkarai, S.-J. Kim, G. Venugopal, Graphene-oxide (GO)–$Fe^{3+}$ hybrid nanosheets with effective sonocatalytic degradation of Reactive Red 120 and study of their kinetics mechanis, Ultrason. Sonochem., 24 (2015) 123-131.

[22] S. Su, W. Guo, C. Yi, Y. Leng, Z. Ma, Degradation of amoxicillin in aqueous solution using sulphate radicals under ultrasound irradiation, Ultrason. Sonochem., 19 (2012) 469-474.

[23] C. Marinescu, M. Ben Ali, A. Hamdi, Y. Cherifi, A. Barras, Y. Coffinier, S. Somacescu, V. Raditoiu, S. Szunerits, R. Boukherroub, Cobalt phthalocyanine-supported reduced graphene oxide: A highly efficient catalyst for heterogeneous activation of peroxymonosulfate for rhodamine B and pentachlorophenol degradation, Chem. Eng. J., 336 (2018) 465-475.

[24] S. Stankovich, D. A. Dikin, R. D. Piner, K. A. Kohlhaas, A. Kleinhammes, Y. Jia, Y. Wu, S. T. Nguyen, R. S. Ruoff, Synthesis of graphene-based nanosheets via chemical reduction of exfoliated graphite oxide, Carbon, 45 (2007) 1558-1565.

[25] D. Zaharie-Butucel, M. Potara, A. M. Craciun, R. Boukherroub, S. Szunerits, S. Astilean, Revealing the structure and functionality of graphene oxide and reduced graphene oxide/pyrene carboxylic acid interfaces by correlative spectral and imaging analysis, Phys. Chem. Chem. Phys., 19 (2017) 16038-16046.

[26] G. V. Buxton, C. L. Greenstock, W. P. Helman, A. B. Ross, Critical review of rate constants for reactions of hydrated electrons, hydrogen atoms and hydroxyl radicals ($^{\cdot}OH/^{\cdot}O^{-}$) in aqueous solution, J. Phys. Chem. Ref. Data, 17 (1988) 513−886.

[27] P. Neta, R. E. Huie, A. B. Ross, Rate constants for reactions of inorganic radicals in aqueous solution, J. Phys. Chem. Ref. Data, 17 (1988) 1027−1284.

[28] G. Wei, X. Liang, Z. He, Y. Liao, Z. Xie, P. Liu, S. Ji, H. He, D. Li, J. Zhang, Heterogeneous activation of Oxone by substituted magnetites $Fe_{3-x}M_xO_4$ (Cr, Mn, Co, Ni) for degradation of Acid Orange II at neutral pH, J. Mol. Catal. A, 398 (2015) 86-94.

[29] W.-D. Oh, Z. Dong, Z.-T. Hu, T.-T. Lim, A novel quasi-cubic $CuFe_2O_4$–$Fe_2O_3$ catalyst prepared at low temperature for enhanced oxidation of bisphenol A *via* peroxymonosulfate activation, J. Mater. Chem. A, 3 (2015) 22208-22217.

[30] B. P. Chaplin, E. Roundy, K. Guy, J. R. Shapley, C. J. Werth, Effects of natural water ions and humic acid on catalytic nitrate reduction kinetics using an alumina supported Pd-Cu catalyst, Environ. Sci. Technol., 40 (2006) 3075-3081.

[31] B. Darsinou, Z. Frontistis, M. Antonopoulou, I. Konstantinou, D. Mantzavinos, Sono-activated persulfate oxidation of bisphenol A: Kinetics, pathways and the controversial role of temperature, Chem. Eng. J., 280 (2015) 623-633.

[32] A. O. Kondrakov, A. N. Ignatev, F. H. Frimmel, S. Bräse, H. Horn, A. I. Revelsky, Formation ofgenotoxic quinones during bisphenol A degradation by TiO2 photocatalysis and UVphotolysis: A comparative study, Appl. Catal. B, 160-161 (2014) 106-114.

[33] J. Choi, M. Cui, Y. Lee, J. Kim, Y. Son, J. Khim, Hydrodynamic cavitation and activated persulfate oxidation for degradation of bisphenol A: Kinetics and mechanism, Chem. Eng. J., 338 (2018) 323-332.

[34] X. Li, Z. Wang, B. Zhang, A. I. Rykov, M. A. Ahmed, J. Wang, $FexCo_{3-x}O_4$ nanocages derived from nanoscale metal–organicframeworks for removal of bisphenol A by activation of peroxymonosulfate, Appl. Catal. B, 181 (2016) 788-799.

[35] C.-Y. Wang, X. Zhang, H.-B. Qiu, W.-K. Wang, G.-X. Huang, J. Jiang, H.-Q. Yu, Photocatalytic degradation of bisphenol A by oxygen-rich and highlyvisible-light responsive $Bi_{12}O_{17}Cl_2$ nanobelts, Appl. Catal. B, 200 (2017) 659-665.

[36] E. Kusvuran, D. Yildirim, Degradation of bisphenol A by ozonation and determination of degradation intermediates by gas chromatography–mass spectrometry and liquid chromatography–mass spectrometry, Chem. Eng. J., 220 (2013) 6-14.

[37] Q. Han, H. Wang, W. Dong, T. Liu, Y. Yin, H. Fan, Degradation of bisphenol A by ferrate(VI) oxidation: Kinetics, products and toxicity assessment, Chem. Eng. J., 262 (2015) 34-40.

[38] F. Minisci, A. Citterio, C. Giordano, Electron-Transfer Processes: Peroxydisulfate, a Useful and Versatile Reagent in Organic Chemistry, Acc. Chem. Res., 16 (1983) 27-32.

[39] M. Molkenthin, T. Olmez-Hanci, M. R. Jekel, I. Arslan-Alaton, Photo-Fenton-like treatment of BPA: Effect of UV light source and water matrix on toxicity and transformation products, Water Res., 47 (2013) 5052-5064.

[40] I. Dalmázio, M. O. Almeida, R. Augusti, T. M. A. Alves, Monitoring the Degradation of Tetracycline by Ozone in Aqueous Medium Via Atmospheric Pressure Ionization Mass Spectrometry, J. Am. Soc. Mass Spectrom., 18 (2007) 679-687.

[41] A. M. Kamel, H. G. Fouda, P. R. Brown, B. Munson, Mass Spectral Characterization of Tetracyclines by Electrospray Ionization, H/D Exchange, and Multiple Stage Mass Spectrometry, J. Am. Soc. Mass Spectrom., 13 (2002) 543-557.

[42] Y. Wang, H. Zhang, J. Zhang, C. Lu, Q. Huang, J. Wu, F. Liu, Degradation of tetracycline in aqueous media by ozonation in an internal loop-lift reactor, J. Hazard. Mater., 192 (2011) 35-43.

[43] H. Shen, J. Wang, J. Jiang, B. Luo, B. Mao, W. Shi, All-solid-state Z-scheme system of RGO-$Cu_2O$/$Bi_2O_3$ for tetracycline degradation under visible-light irradiation, Chem. Eng. J., 313 (2017) 508-517.

[44] D. Fu, Z. Chen, D. Xia, L. Shen, Y. Wang, Q. Li, A novel solid digestate-derived biochar-Cu NP composite activating $H_2O_2$ system for simultaneous adsorption and degradation of tetracycline, Environm. Pollut., 221 (2017) 301-310.

[45] Y. Liu, X. He, Y. Fu, D. D. Dionysiou, Kinetics and mechanism investigation on the destruction ofoxytetracycline by UV-254 nm activation of persulfate, J. Hazard. Mater., 305 (2016) 229-239.

[46] Y.-Y. Chen, Y.-L. Ma, J. Yang, L.-Q. Wang, J.-M. Lv, C.-J. Ren, Aqueous tetracycline degradation by $H_2O_2$ alone: Removal and transformation pathway, Chem. Eng. J., 307 (2017) 15-23.

[47] J. Wang, D. Zhi, H. Zhou, X. He, D. Zhang, Evaluating tetracycline degradation pathway and intermediate toxicity during the electrochemical oxidation over a $Ti/Ti_4O_7$ anode, Water Res., 137 (2018) 324-334.

[48] J. Niu, S. Ding, L. Zhang, J. Zhao, C. Feng, Visible-light-mediated Sr-Bi2O3 photocatalysis of tetracycline: Kinetics, mechanisms and toxicity assessment, Chemosphere, 93 (2013) 1-8.

**Figure captions**

**Figure 1**: UV-vis absorption spectra of initial GO (**a**), and rGO (**b**).

**Figure 2**: Raman spectra of GO (**a**), as-prepared rGO before (**b**) and after reaction with 0.3 mM PMS for 3 h under ultrasonication (**c**).

**Figure 3**: High resolution XPS spectrum of the $C_{1s}$ region of reduced graphene oxide (rGO) before (**a**) and after reaction with 0.3 mM PMS for 3 h under ultrasonication (**b**).

**Figure 4:** High resolution transmission microscopy (HRTEM) and energy-dispersive X-ray (EDX) analysis of rGO.

**Figure 5:** RhB (20 µM) degradation efficiency using different oxidation conditions ([rGO]=0.25 mg/mL, [PMS]=0.3 mM).

**Figure 6**: (**A**) Influence of rGO (0.25 and 0.50 mg/mL) + PMS (0.3 mM) on RhB (20 µM) degradation under utrasonication for 20 min; (**B**) Influence of PMS concentration (0.1, 0.2 and 0.3 mM) + rGO (0.25 mg/mL) on RhB (20 µM) degradation under ultrasonication; (**C**) Performance of the rGO/PMS system for the removal of RhB at different concentrations (20, 30, and 40 µM) under ultrasonication, [rGO]=0.25 mg/mL and [PMS]=0.3 mM.

**Figure 7:** TOC removal efficiency of RhB, BPA and TC using rGO/PMS system under ultrasonication.

**Figure 8**: Repeated recycling of rGO with PMS for the degradation of RhB ([rGO]: 0.25 mg/mL; [RhB]: 20 µM; [PMS]: 0.3 mM) under ultrasonication (35 KHz).

**Figure 9**: Effect of ethanol (EtOH) and *tert*-butanol (TBA) as radical scavengers for the degradation of RhB (20 µM) using rGO (0.25 mg/L) and PMS (0.3 mM) under ultrasonication, [EtOH]=0.2 M and [TBA]=0.2 M.

**Figure 10**: EPR spectra of rGO and rGO/PMS recorded at room temperature.

**Figure 11**: EPR spectra of spin adduct formed after 1 min (**A**), and experimental and simulated spectra after respectively 10 and 20 min. The stars denote the DMPO-oxidized species.

**Figure 12:** (**A**) BPA (100 µM) degradation efficiency using different oxidation conditions under ultrasonication, (**B**) Effect of different water matrix species on the BPA (100 µM) degradation ([rGO]=0.25 mg/mL, [PMS]=1 mM) under ultrasonication.

**Figure 13:** LC-MS chromatograms of BPA (100 µM) + rGO (0.25 mg/mL)/PMS (1 mM) before and after addition of rGO (1 mg/mL) under ultrasonication for 0, 20, 30 and 40 min.

**Figure 14:** Plausible BPA degradation pathway upon catalytic reaction with rGO/PMS under ultrasonication.

**Figure 15:** TC (100 µM) degradation efficiency using different oxidation conditions ([rGO]=0.25 mg/mL, [PMS]=1 mM) under ultrasonication.

**Figure 16:** LC-MS chromatograms of TC (100 µM) + PMS (1 mM) before and after (red) addition of rGO (1 mg/mL) under ultrasonication for 0, 15, 20 and 30 min.

**Figure 17:** Plausible TC degradation pathway upon catalytic reaction with rGO/PMS under ultrasonication.

**Table 1**. Mn composition obtained by ICP-OES analysis.

| **Sample** | **Mn (wt%)** |
|---|---|
| GO | 1.88 |
| rGO | 1.89 |
| rGO-acid* | 0.22 |
| rGO-acid** | 0.04 |

*treated with $HNO_3/H_2SO_4$ (1/1) at 80 °C for 24 h

** treated with $HNO_3/H_2SO_4$ (1/1) at 80 °C for 48 h

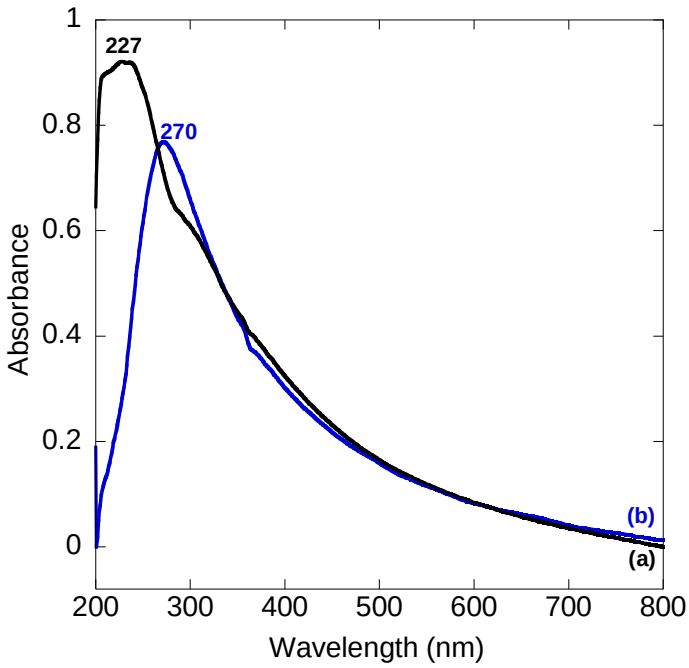
227
270
(b)
(a)
Absorbance
Wavelength (nm)
1
0.8
0.6
0.4
0.2
0
200
300
400
500
600
700
800

**Figure 1**

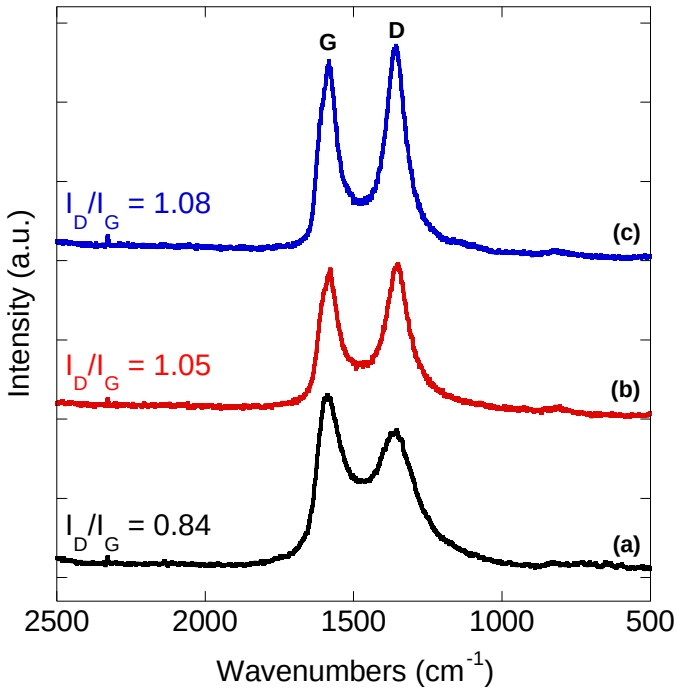
G
D
I_D/I_G = 1.08
(c)
I_D/I_G = 1.05
(b)
I_D/I_G = 0.84
(a)
Intensity (a.u.)
2500
2000
1500
1000
500
Wavenumbers (cm-1)

**Figure 2**

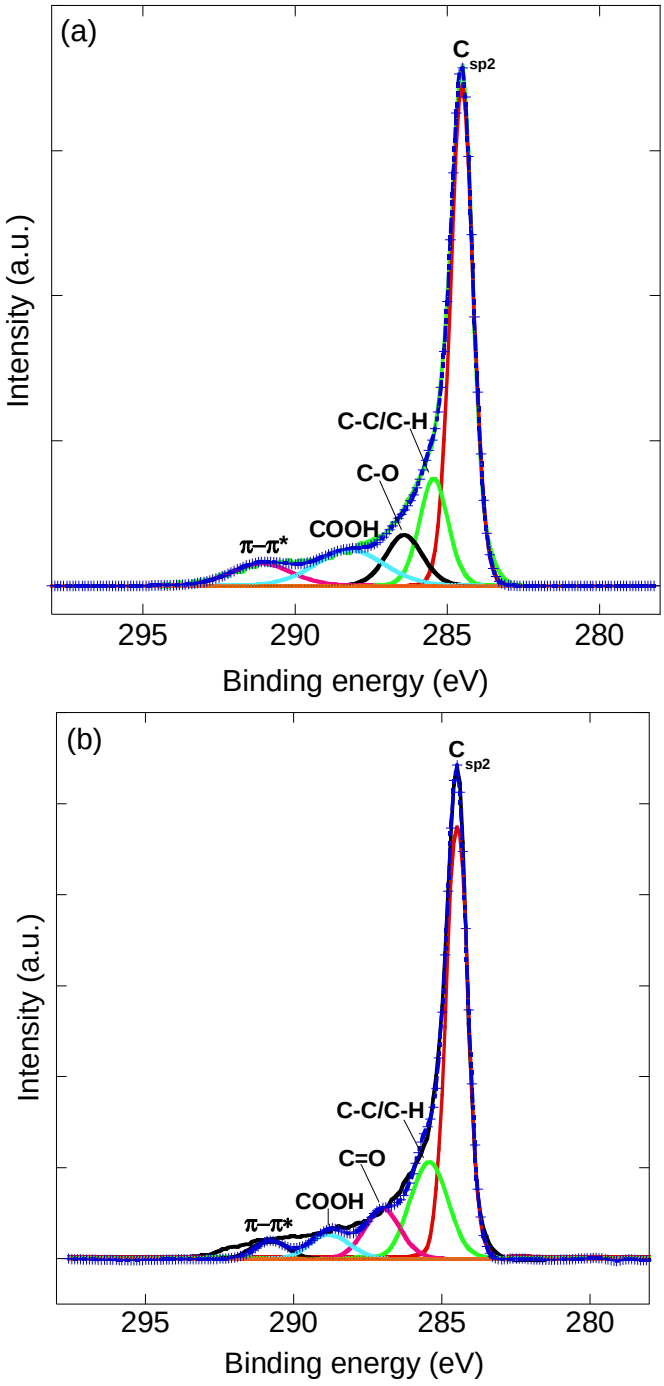
(a)
C sp2
C-C/C-H
C-O
COOH
π–π*
Intensity (a.u.)
295
290
285
280
Binding energy (eV)
(b)
C sp2
C-C/C-H
C=O
COOH
π–π*
Intensity (a.u.)
295
290
285
280
Binding energy (eV)

**Figure 3**

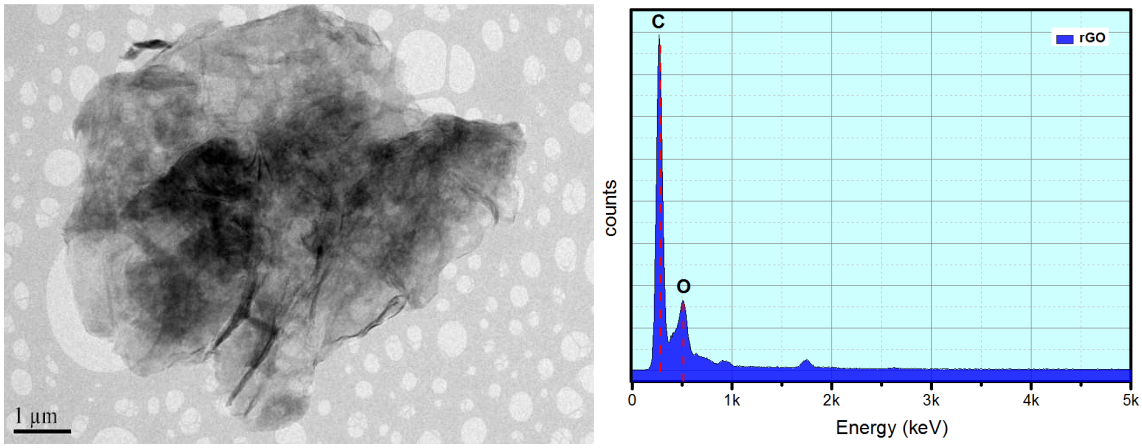


**Figure 4**

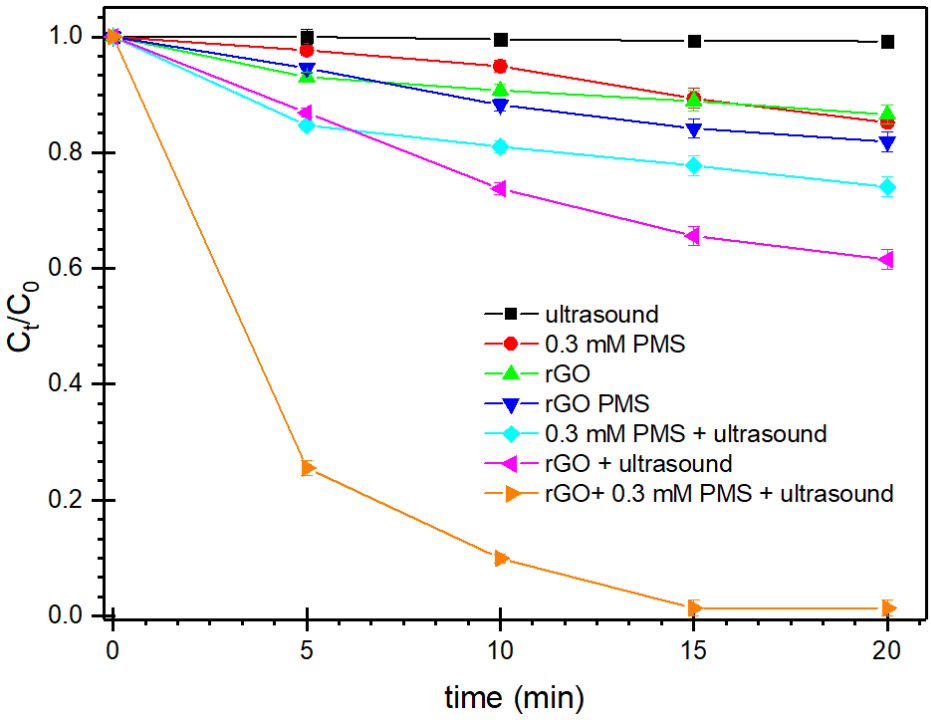
1.0
0.8
0.6
0.4
0.2
0.0
$C_t/C_0$
0
5
10
15
20
time (min)
ultrasound
0.3 mM PMS
rGO
rGO PMS
0.3 mM PMS + ultrasound
rGO + ultrasound
rGO+ 0.3 mM PMS + ultrasound

**Figure 5**

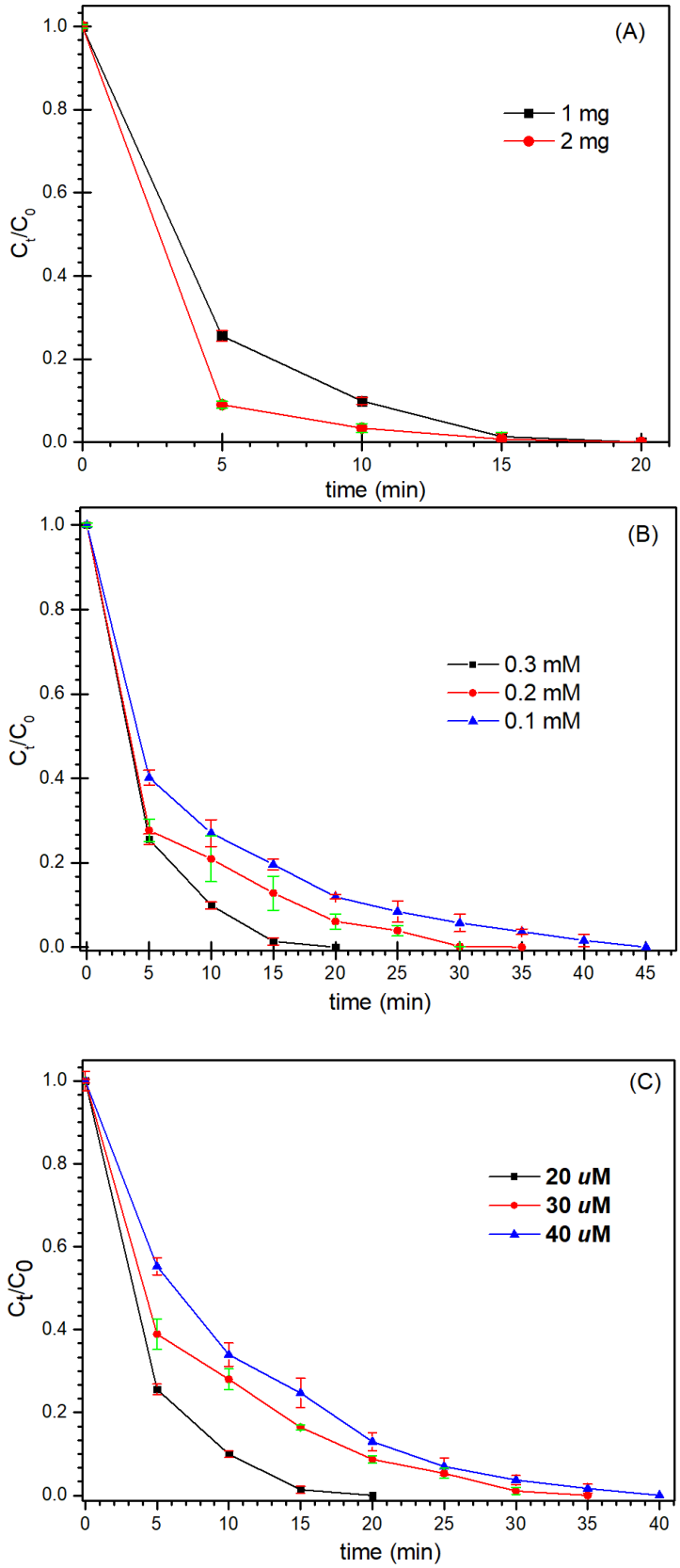
(A)
1 mg
2 mg
$C_t/C_0$
time (min)
(B)
0.3 mM
0.2 mM
0.1 mM
$C_t/C_0$
time (min)
(C)
20 uM
30 uM
40 uM
$C_t/C_0$
time (min)

**Figure 6**

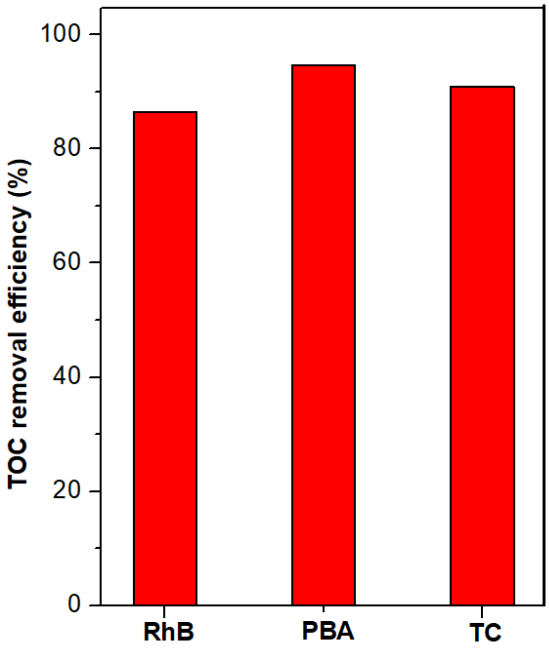


**Figure 7**

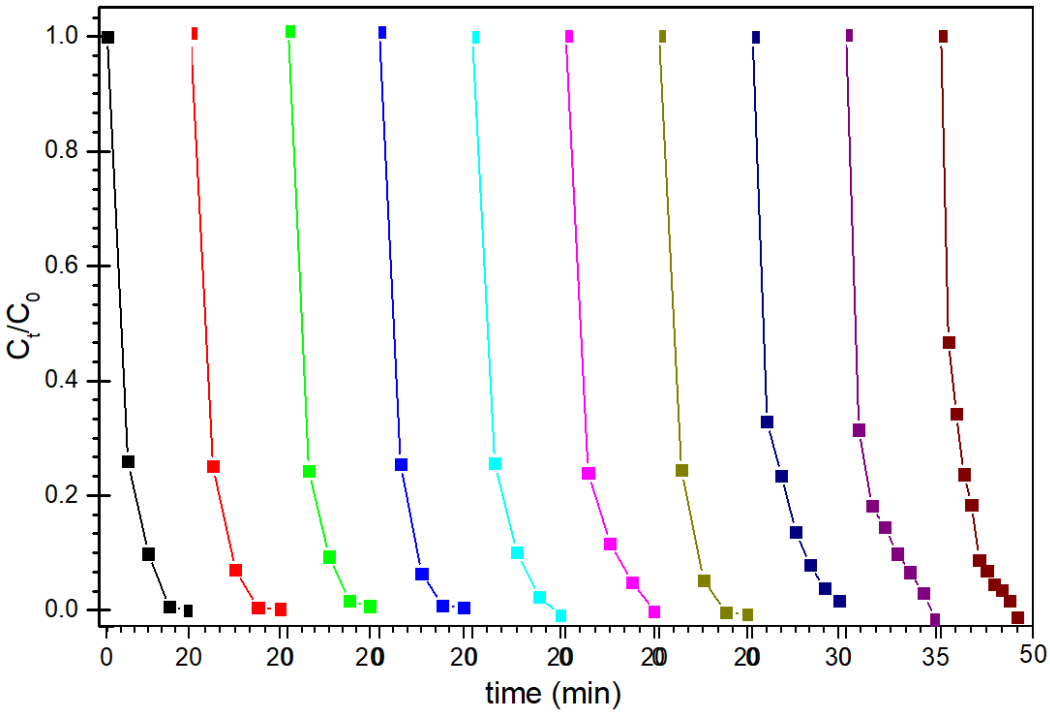


**Figure 8**

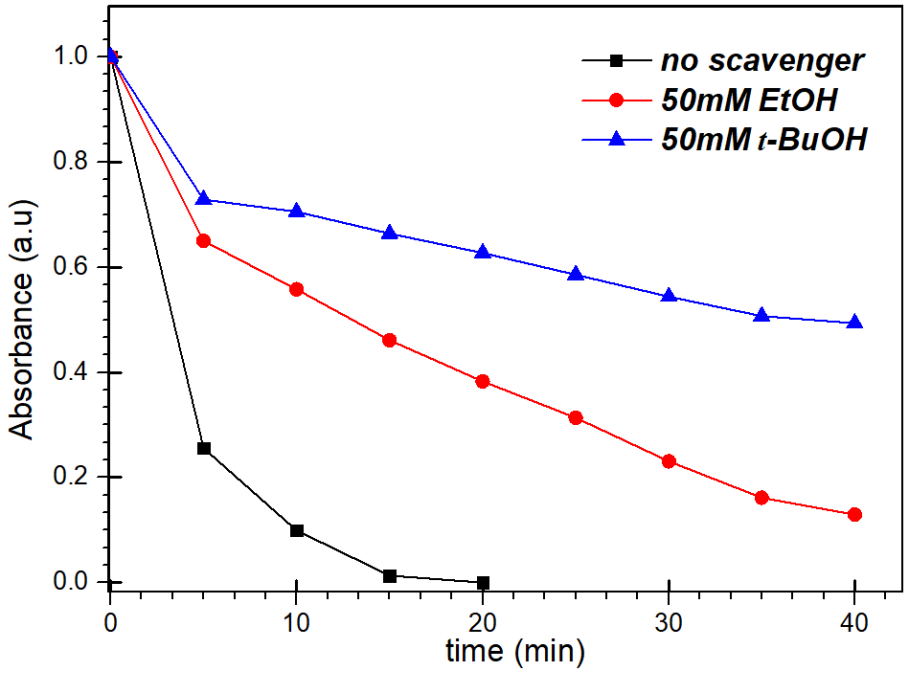
no scavenger
50mM EtOH
50mM t-BuOH
Absorbance (a.u)
time (min)
0.0
0.2
0.4
0.6
0.8
1.0
0
10
20
30
40

**Figure 9**

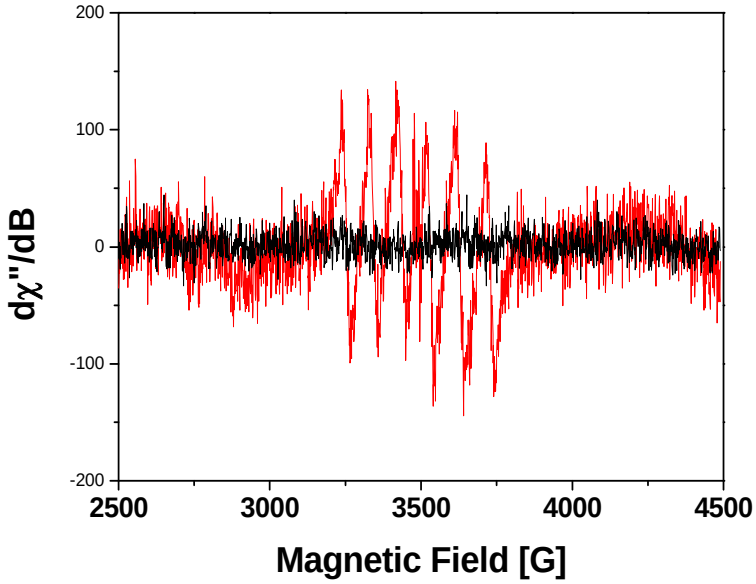
200
100
0
-100
-200
dχ"/dB
2500
3000
3500
4000
4500
Magnetic Field [G]

**Figure 10**

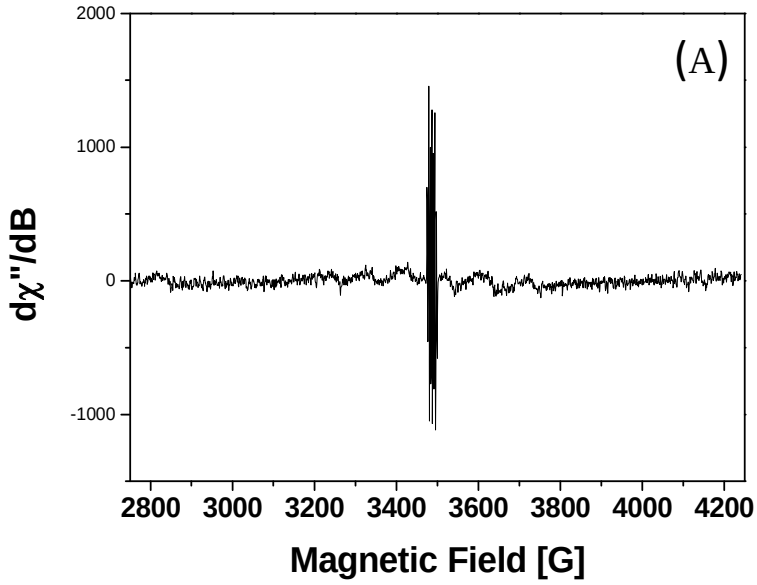
(A)
2000
1000
0
-1000
dχ"/dB
2800
3000
3200
3400
3600
3800
4000
4200
Magnetic Field [G]

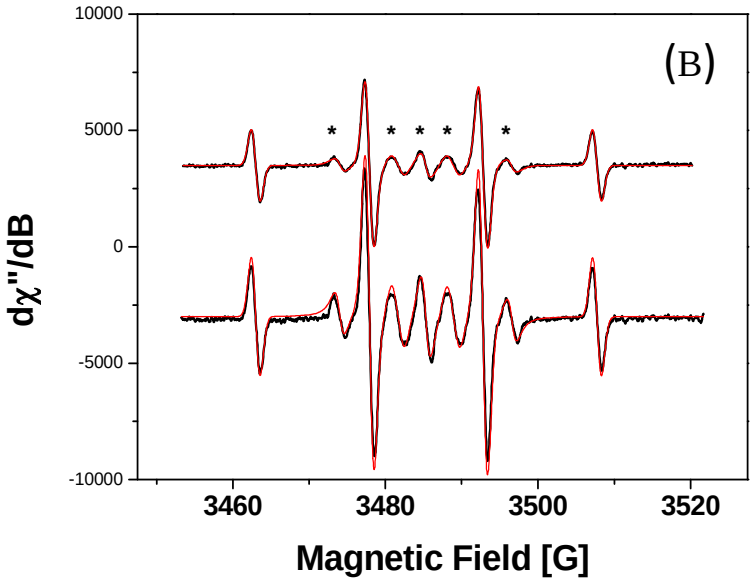
(B)
10000
5000
0
-5000
-10000
dχ"/dB
*
*
*
*
*
3460
3480
3500
3520
Magnetic Field [G]

**Figure 11**

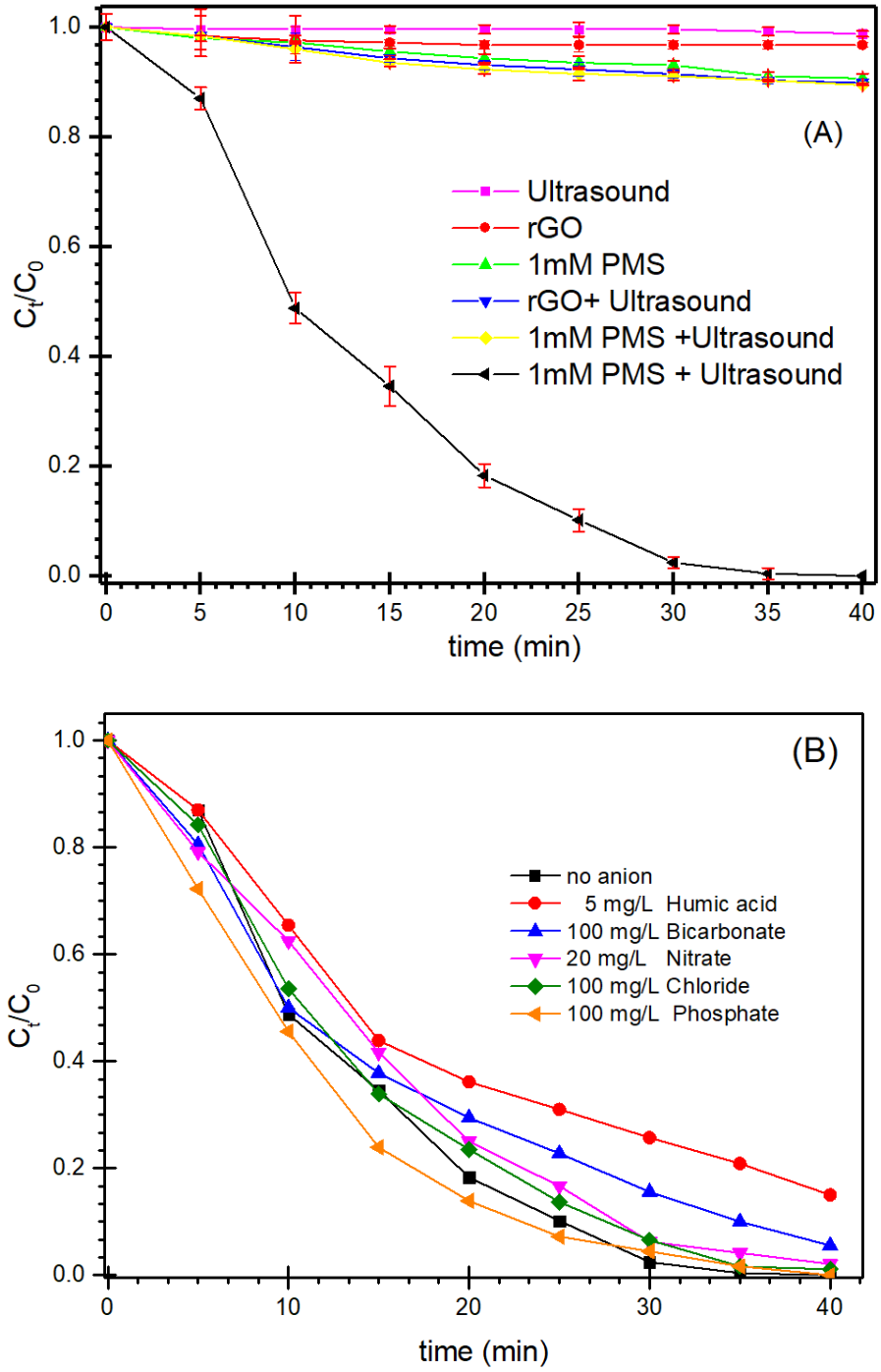
(A)
Ultrasound
rGO
1mM PMS
rGO+ Ultrasound
1mM PMS +Ultrasound
1mM PMS + Ultrasound
$C_t/C_0$
time (min)
(B)
no anion
5 mg/L Humic acid
100 mg/L Bicarbonate
20 mg/L Nitrate
100 mg/L Chloride
100 mg/L Phosphate
$C_t/C_0$
time (min)

**Figure 12**

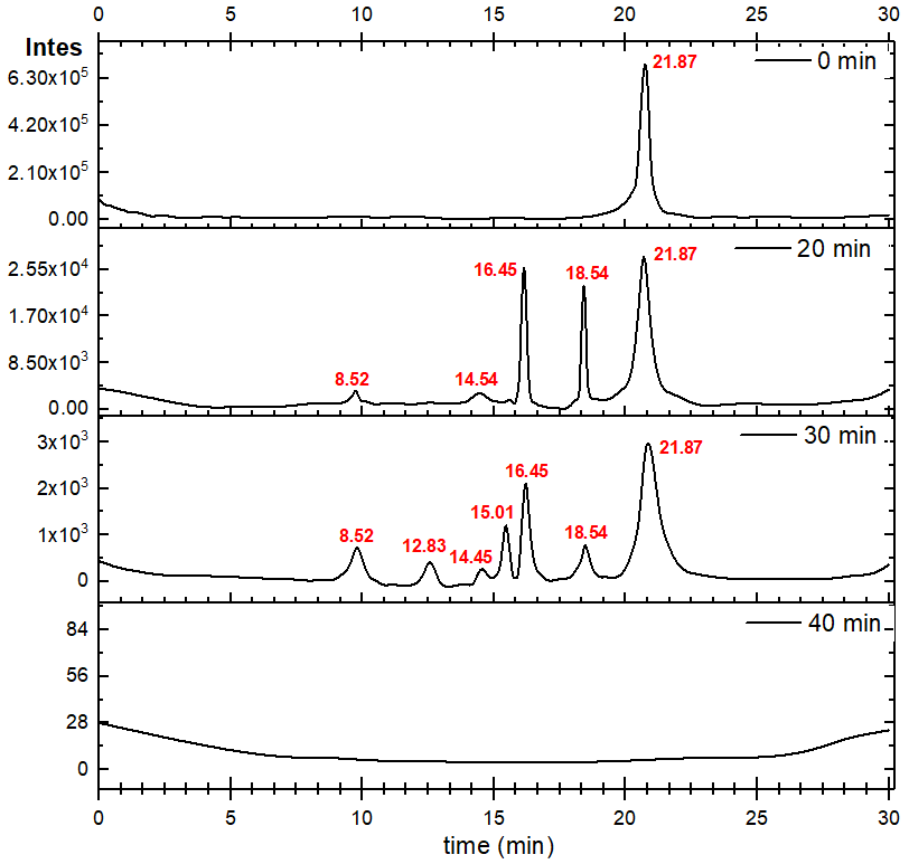
Intes
6.30x10^5
4.20x10^5
2.10x10^5
0.00
0 min
21.87
2.55x10^4
1.70x10^4
8.50x10^3
0.00
20 min
16.45
18.54
21.87
8.52
14.54
3x10^3
2x10^3
1x10^3
0
30 min
21.87
16.45
15.01
8.52
12.83
14.45
18.54
84
56
28
0
40 min
0
5
10
15
20
25
30
time (min)

**Figure 13**

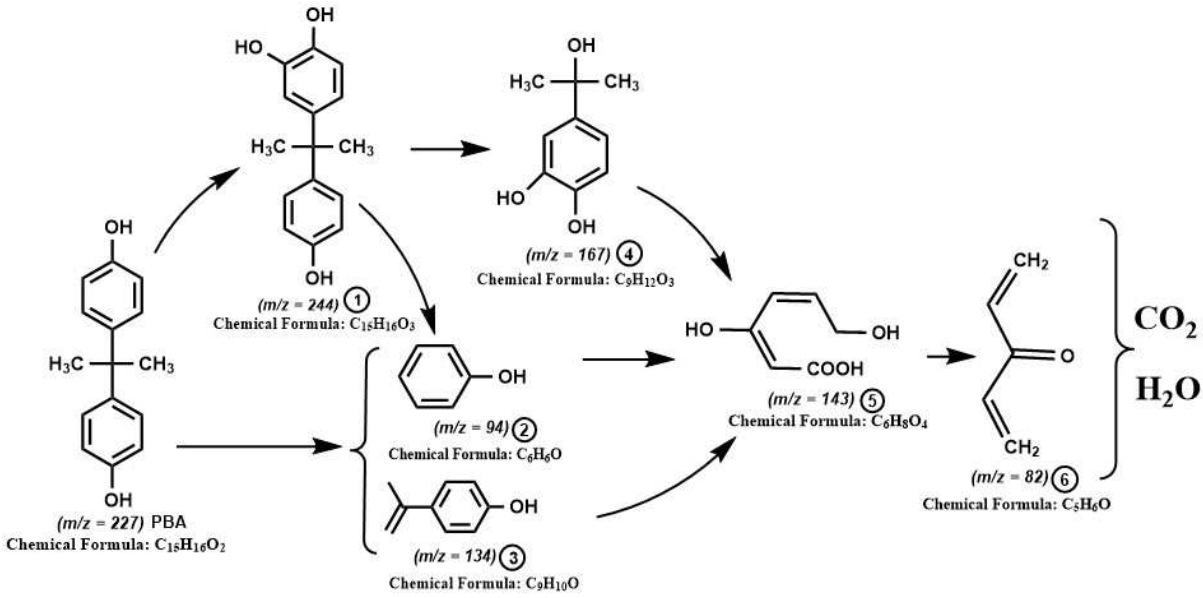
OH
HO
H3C
CH3
OH
(m/z = 244) 1
Chemical Formula: C15H16O3
OH
H3C
CH3
HO
OH
(m/z = 167) 4
Chemical Formula: C9H12O3
OH
H3C
CH3
OH
(m/z = 227) PBA
Chemical Formula: C15H16O2
OH
(m/z = 94) 2
Chemical Formula: C6H6O
OH
(m/z = 134) 3
Chemical Formula: C9H10O
HO
OH
COOH
(m/z = 143) 5
Chemical Formula: C6H8O4
CH2
O
CH2
(m/z = 82) 6
Chemical Formula: C5H6O
CO2
H2O

**Figure 14**

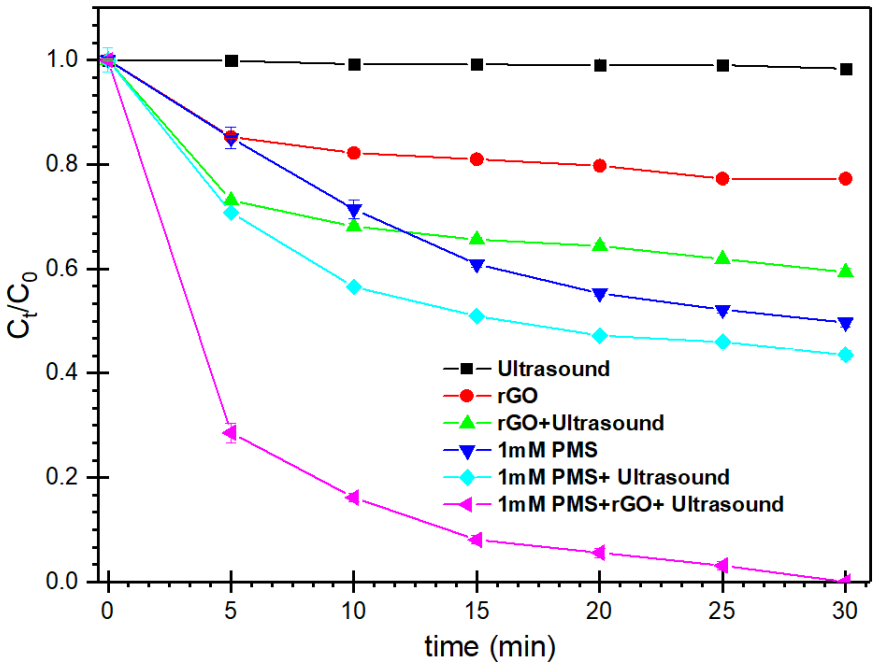
1.0
0.8
0.6
0.4
0.2
0.0
$C_t/C_0$
0
5
10
15
20
25
30
time (min)
Ultrasound
rGO
rGO+Ultrasound
1mM PMS
1mM PMS+ Ultrasound
1mM PMS+rGO+ Ultrasound

**Figure 15**

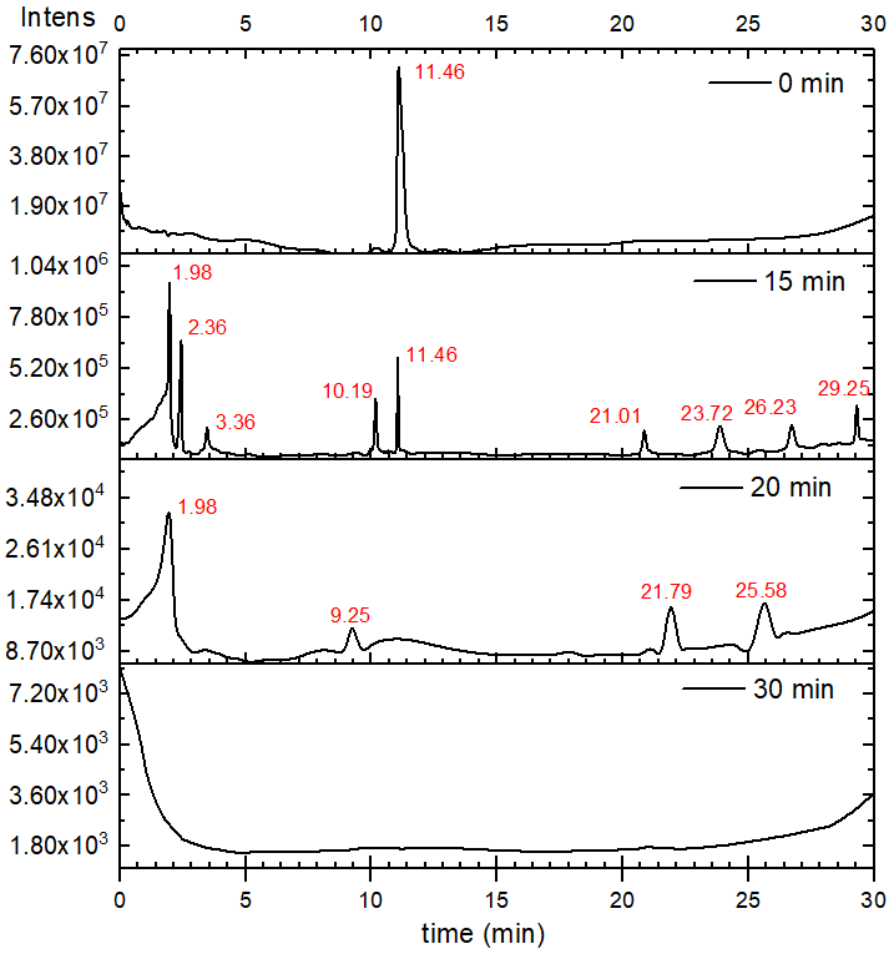
Intens
7.60x10^7
5.70x10^7
3.80x10^7
1.90x10^7
1.04x10^6
7.80x10^5
5.20x10^5
2.60x10^5
3.48x10^4
2.61x10^4
1.74x10^4
8.70x10^3
7.20x10^3
5.40x10^3
3.60x10^3
1.80x10^3
0 min
15 min
20 min
30 min
11.46
1.98
2.36
3.36
10.19
11.46
21.01
23.72
26.23
29.25
1.98
9.25
21.79
25.58
0
5
10
15
20
25
30
time (min)

**Figure 16**

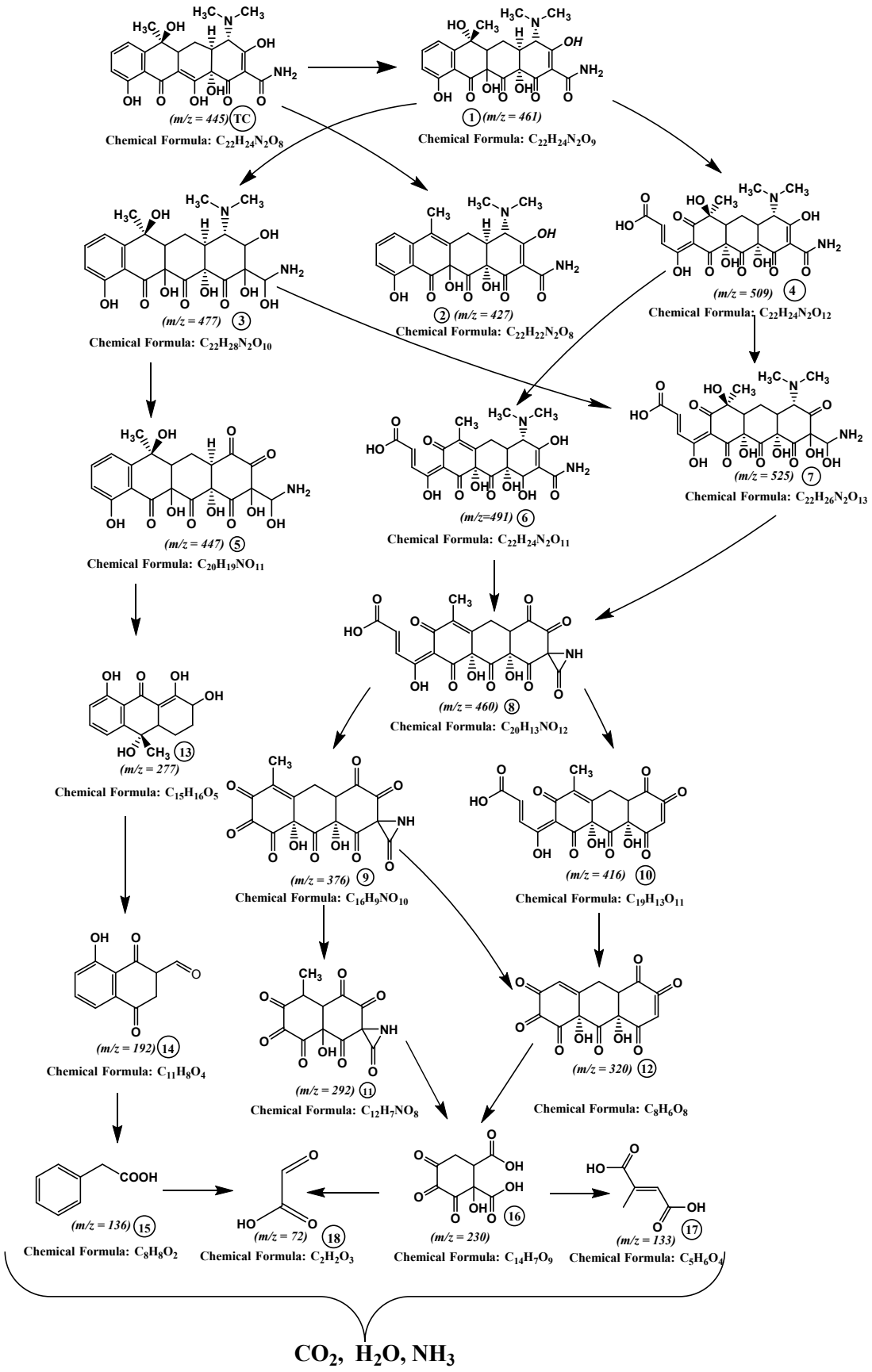
(m/z = 445) TC
Chemical Formula: C22H24N2O8
1 (m/z = 461)
Chemical Formula: C22H24N2O9
2 (m/z = 427)
Chemical Formula: C22H22N2O8
3 (m/z = 477)
Chemical Formula: C22H28N2O10
4 (m/z = 509)
Chemical Formula: C22H24N2O12
5 (m/z = 447)
Chemical Formula: C20H19NO11
6 (m/z=491)
Chemical Formula: C22H24N2O11
7 (m/z = 525)
Chemical Formula: C22H26N2O13
8 (m/z = 460)
Chemical Formula: C20H13NO12
13 (m/z = 277)
Chemical Formula: C15H16O5
9 (m/z = 376)
Chemical Formula: C16H9NO10
10 (m/z = 416)
Chemical Formula: C19H13O11
14 (m/z = 192)
Chemical Formula: C11H8O4
11 (m/z = 292)
Chemical Formula: C12H7NO8
12 (m/z = 320)
Chemical Formula: C8H6O8
15 (m/z = 136)
Chemical Formula: C8H8O2
18 (m/z = 72)
Chemical Formula: C2H2O3
16 (m/z = 230)
Chemical Formula: C14H7O9
17 (m/z = 133)
Chemical Formula: C5H6O4
CO2, H2O, NH3

**Figure 17**